Inorganic Chemistry

Article

pubs.acs.org/IC

Spin-Crossover Behavior in Two New Supramolecular Isomers

Zheng Yan,[†] Zhao-Ping Ni,[†] Fu-Sheng Guo,[†] Jin-Yan Li,[†] Yan-Chong Chen,[†] Jun-Liang Liu,[†] Wei-Quan Lin,[†] Daniel Aravena,[‡] Eliseo Ruiz,*[,‡] and Ming-Liang Tong*[,†]

[†]Key Laboratory of Bioinorganic and Synthetic Chemistry of Ministry of Education, State Key Laboratory of Optoelectronic Materials and Technologies, School of Chemistry and Chemical Engineering, Sun Yat-Sen University, 135 Xingang Road West, Guangzhou 510275, P. R. China

[‡]Departament de Química Inorgànica and Institut de de Recerca de Química Teòrica i Computacional, Universitat de Barcelona, Diagonal 645, 08028 Barcelona, Spain

Supporting Information

ABSTRACT: Two spin-crossover (SCO) supramolecular isomers formulated as $[Fe(Mebpt)\{Au(CN)_2\}]_n \cdot xH_2O$ (**1**, $x = 0$, and **2**·H_2O, $x = n$, MebptH = 3-(5-methyl-2-pyridyl)-5-(2-pyridyl)-1,2,4-triazole) have been successfully isolated and characterized by single-crystal X-ray crystallography, thermogravimetric analysis, differential scanning calorimetry, variable-temperature powder X-ray diffraction, and magnetic measurements. Structural analysis reveals that **1** is a two-dimensional coordination layer and **2**·H_2O is a one-dimensional coordination ladder structure, in which the $Mebpt^-$ ligands are coordinated in *trans* and *cis* bridging mode in **1** and **2**·H_2O, respectively. Dramatically, their SCO properties are further influenced by the octahedral coordination configuration of Fe(II). In **1**, only the Fe(II) centers in *trans* configuration exhibit spin transition (T_c = 303 K), while in **2**·H_2O and the dehydrated **2**, gradual two-step SCO (T_{c1} = 235 K, T_{c2} = 313 K) and one-step SCO behaviors (T_c = 315 K) occur, respectively.

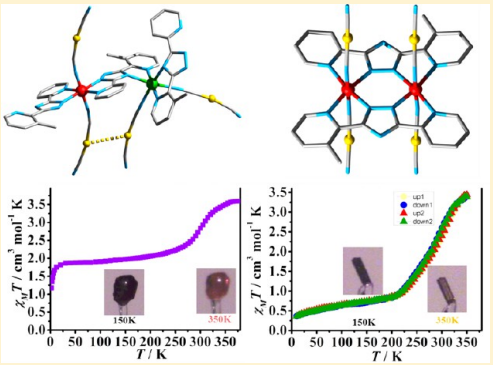

INTRODUCTION

In response to external stimuli such as temperature, pressure, light, and guest molecules, the electronic configurations of spin-crossover (SCO) complexes are switchable between the high spin (HS) and low spin (LS) states.[1] These characters of SCO materials offer attractive opportunities for the applications in sensing, memory, and display devices.[2−6] However, to date a general structure−property correlation for understanding the essence of SCO has yet to be defined. In this regard, it would be fruitful to investigate closely related SCO molecules with subtle structural changes, preferably those with supramolecular isomerism or polymorphism.[7] A recent review summarized that polymorphism in most SCO systems[8] is numbered and mostly mononuclear, which is mainly formed due to different crystal packing and/or configurations of ligand. The SCO stereoisomers (*cis*:*trans*) are even unusual because metal complexes with different geometries rarely possess similar crystallization kinetics.[9a] To the best of our knowledge, there is only one case of SCO active stereoisomers in cocrystallized mononuclear complexes;[9b] however, no SCO example coexisting with *cis* and *trans* configurations in the coordination polymers has been reported.

As a continuation of our study on triazole-bipyridine system, we choose the 3-(5-methyl-2-pyridyl)-5-(2-pyridyl)-1,2,4-triazole (MebptH) and $KAu(CN)_2$ ligand mainly for the following reasons: (1) As a variant of the well-studied 4-substituted 3,5-di(2-pyridyl)-1,2,4-triazole ligand (2,2-Rbpt), it should also provide an appropriate ligand field favoring the occurrence of SCO.[10] (2) The $Mebpt^-$ ligand can take on *cis* and *trans* bridging modes (Scheme 1),[7b] resulting in a variety of isomers for the investigation of the structure−property correlation. (3) With bridging by the linear $Au(CN)_2^-$ unit, the cooperation effect can be enhanced by constructing the $[Fe(Mebpt)]^+$ motifs into a coordination polymer. Previously, a few SCO coordination frameworks formulated as $[Fe(L)\{Au(CN)_2\}]\cdot G$ (L = pyridine analogue)[11] have been reported. Recently, Real and co-workers reported a novel 3D Fe(II) SCO coordination polymer based on the bis-triazole and $[Au(CN)_2]^-$ ligands, which displayed spin transition.[12] Herein, we report two

Scheme 1. *Trans* (a) and *Cis* (b) Bridging Modes of $Mebpt^-$ Ligand in 1 and 2·H_2O

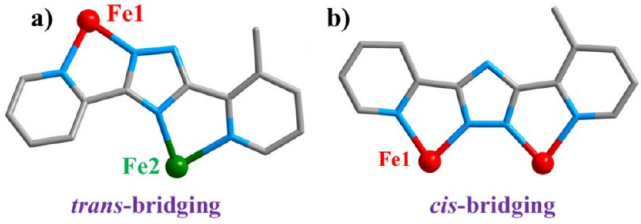

Received: August 15, 2013
Published: December 23, 2013

   dx.doi.org/10.1021/ic402096s | *Inorg. Chem.* 2014, 53, 201−208

Table 1. Summary of the Crystal Data and Structure Refinement Parameters for 1 and 2·H_2O

	1			2·H_2O		
	T = 150 K	T = 298 K	T = 373 K	T = 150 K	T = 275 K	T = 350 K
color	black	dark red	red	black	light red	yellow
formula	$C_{15}H_{10}AuFeN_7$	$C_{15}H_{10}AuFeN_7$	$C_{15}H_{10}AuFeN_7$	$C_{15}H_{12}AuFeN_7O$	$C_{15}H_{12}AuFeN_7O$	$C_{15}H_{12}AuFeN_7O$
fw	541.12	541.12	541.12	559.12	559.12	559.12
space group	$C2/c$	$C2/c$	$C2/c$	$P\bar{1}$	$P\bar{1}$	$P\bar{1}$
a/Å	14.4588(14)	14.5730(18)	14.5393(19)	9.3277(16)	9.3970(17)	9.616(5)
b/Å	10.9079(9)	11.0366(12)	11.0615(15)	10.1541(13)	10.3248(16)	10.473(5)
c/Å	21.423(2)	21.694(3)	21.854(3)	10.8491(17)	10.9108(16)	10.9906(6)
α/deg	90	90	90	106.128(4)	103.937(4)	104.535(13)
β/deg	101.441(2)	101.854(3)	102.012(3)	102.779(5)	102.971(5)	103.124(13)
γ/deg	90	90	90	112.248(4)	112.799(5)	112.617(11)
V/Å^3	3311.6(5)	3414.7(7)	3437.7(8)	849.9(2)	885.4(2)	914.8(8)
Z	8	8	8	2	2	2
D_{calcd}/g cm^{-3}	2.171	2.105	2.091	2.177	2.097	2.030
reflns collected	3202	3243	3299	3885	3408	3512
reflns unique	2153	2111	1698	2788	1668	1584
R_{int}	0.1507	0.0865	0.1400	0.0698	0.0616	0.0673
GOF	0.991	1.062	1.034	1.061	0.963	0.966
R1[a] [$I > 2\sigma(I)$]	0.0524	0.0698	0.0704	0.0711	0.0608	0.0808
wR2[b] (all data)	0.1270	0.1655	0.2244	0.1924	0.1982	0.2425

[a] $R1 = \sum||F_o| - |F_c||/\sum|F_o|$. [b] $wR2 = \{[\sum w(F_o^2 - F_c^2)^2]/\sum[w(F_o^2)^2]\}^{1/2}$.

isomeric coordination polymers formulated as $[Fe(Mebpt)\{Au(CN)_2\}]_n \cdot xH_2O$ (**1**, $x = 0$, and **2**·H_2O, $x = n$), which exhibit near room temperature SCO behaviors. To the best of our knowledge, **1** is the first case of a 2D SCO coordination polymer with the Fe^{II} in both *cis* and *trans* coordination configurations, while **2**·H_2O is a rare SCO coordination polymer example with a 1D coordination ladder structure. Moreover, **2**·H_2O and the dehydrated complex **2** exhibit gradual two-step (T_{c1} = 235 K, T_{c2} = 313 K) and one-step SCO behaviors (T_c = 315 K), respectively.

EXPERIMENTAL SECTION

Materials and General Procedures. The MebptH and K[$Au(CN)_2$] ligands were obtained from Jinan Camolai Trading company and used without further purification. All other compounds and reagents were obtained commercially and used as received. UV−vis spectra were performed on crystal samples of **1** and **2**·H_2O using a Cary 5000 UV−vis−NIR spectrophotometer. Infrared spectra were recorded in KBr tablets in the range 4000−400 cm^{-1} with a Bruker-tensor 27 spectrometer. The C, H, and N elemental analyses of the crystal samples were performed on an Elementar Vario EL elemental analyzer. Thermogravimetric (TG) analyses were carried out on crystal samples of **2**·H_2O and **2** using NETZSCH TG209F3 thermogravimetric analyzer instrument under nitrogen at a scan rate of 10 K min^{-1} in heating modes. Differential scanning calorimetry (DSC) measurements were carried out on crystal samples of **1**, **2**·H_2O, and **2** using a Netzsch DSC 204 F1 Phoenix instrument under nitrogen at a scan rate of 5 K min^{-1} in both heating and cooling modes. Powder X-ray diffraction (PXRD) intensities of **1** and **2**·H_2O were measured on a D8 ADVANCE X-ray Diffractometer (Cu Kα = 1.540 56 Å). Temperature-dependent magnetic susceptibility data for complexes of **1**, **2**·H_2O, and **2** were obtained using a Quantum Design MPMS-XL-7 SQUID magnetometer under an applied field of 1000 Oe over the temperature range. The samples were packed into plastic films, which were then mounted in low-background diamagnetic plastic straws. The data were corrected for the magnetization of the sample holder and the diamagnetism of the constituent atoms using Pascal constants. All crystal samples characterized by PXRD (Supporting Information Figures S1 and S2), elemental analyses, DSC, and magnetic studies were obtained from the same batch.

Synthesis. *$[Fe(Mebpt)\{Au(CN)_2\}]_n$ (**1**).* A solution of $FeSO_4 \cdot 7H_2O$ (0.028 g, 0.1 mmol), MebptH (0.084 g, 0.1 mmol), and K[$Au(CN)_2$] (0.032 g, 0.1 mmol) in ethanol (8 mL) and water (1 mL) was sealed in a 15 mL Teflon-lined reactor and heated at 120 °C for 3 days, and then cooled to room temperature at a rate of 5 °C/h. Subsequently, dark red block crystals and a small amount of yellow prism crystals along with red amorphous powder were thoroughly washed by ethanol and collected by filtration. The dark red crystals were manually separated under a microscope, with a yield ∼10% of pure crystals based on $FeSO_4 \cdot 7H_2O$. IR (KBr pellet, cm^{-1}): 3070 (m), 2167 (s), 1588 (s), 1467 (w), 1395 (m), 1244 (w), 1120 (s), 1002(w), 802 (w), 629 (w), 572 (w), 512 (w), 465 (w), 442 (m). Anal. Calcd (%) for **1**: C, 33.29; H, 1.86; N, 18.12. Found (%): C, 32.96; H, 1.91; N, 17.76.

*$[Fe(Mebpt)\{Au(CN)_2\}]_n \cdot nH_2O$ (**2**·H_2O).* A solution of $FeSO_4 \cdot 7H_2O$ (0.028 g, 0.1 mmol), MebptH (0.084 g, 0.1 mmol), and K[$Au(CN)_2$] (0.032 g, 0.1 mmol) in ethanol (6 mL) and water (2 mL) was sealed in a 15 mL Teflon-lined reactor and heated at 110 °C for 3 days, and then cooled to room temperature at a rate of 5 °C/h. Subsequently, yellow prism crystals and a small amount of dark red block crystals along with orange-yellow amorphous powder were obtained, and they were thoroughly washed by ethanol and collected by filtration. The yellow prism crystals were manually separated under a microscope, with a yield ∼8% of pure crystals based on $FeSO_4 \cdot 7H_2O$. IR (KBr pellet, cm^{-1}): 3070 (m), 2167 (s), 1588 (s), 1467 (w), 1395 (m), 1244 (w), 1120 (s), 1002(w), 802 (w), 629 (w), 572 (w), 512 (w), 465 (w), 442 (m). Anal. Calcd (%) for **2**·H_2O: C, 32.22; H, 2.16; N, 17.54. Found (%): C, 31.63; H, 2.03; N, 17.28.

*$[Fe(Mebpt)\{Au(CN)_2\}]_n$ (**2**).* Crystals of **2**·H_2O were heated to 593 at 10 K min^{-1} for 30 min and then cooled to room temperature under N_2 atmosphere. Anal. Calcd (%) for **2**: C, 33.29; H, 1.86; N, 18.12. Found (%): C, 32.75; H, 1.95; N, 17.82.

X-ray Structure Determination. Diffraction data for complex **1** was recorded at 150(2), 298(2), and 373(2) K, and for **2**·H_2O at 150(2), 275(2) and 350(2) K, on a Rigaku R-AXIS SPIDER Image Plate diffractometer with graphite-monochromated Mo Kα radiation (λ = 0.710 73 Å). The structures were solved by direct methods, and all non-hydrogen atoms were refined anisotropically by least-squares on F^2 using the SHELXTL program.[14a] Hydrogen atoms on organic ligands were generated by the riding mode. Electron density contributions from disordered water molecules were handled using the SQUEEZE procedure[14b] from the PLATON software.[14c] A summary of the crystallographic data and refinement parameters is

dx.doi.org/10.1021/ic402096s | Inorg. Chem. 2014, 53, 201−208

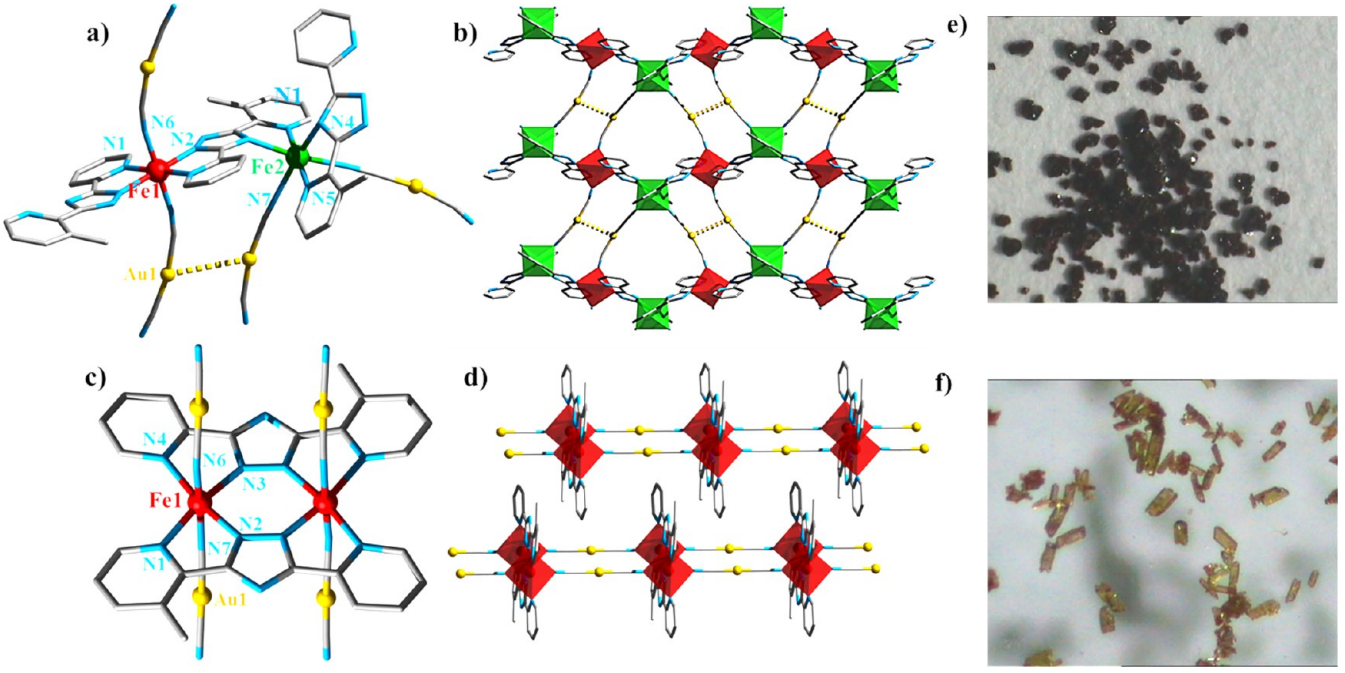

Figure 1. Structure illustrations of **1** and **2**·H_2O: coordination geometries **1** (a) and **2**·H_2O (c); a corrugated 2D layer of **1** (b); a 1D ladder-like chain of **2**·H_2O (d). Color code: N, blue; C, gray; Fe1, red; Fe2, green; Au, orange. Photographs of **1** (e) and **2**·H_2O (f). Hydrogen atoms and H_2O guests are omitted for clarity.

provided in Table 1. CCDC 934369 (1_150K), 934370 (**1**_298K), 934371 (**1**_373K), 934372 (**2**·H_2O_150K), 934373 (**2**·H_2O_275K), 934374 (**2**·H_2O_350K) contain the supplementary crystallographic data for this paper. These data can be obtained free of charge from the Cambridge Crystallographic Data Center via www.ccdc.cam.ac.uk/data_request/cif.

RESULTS AND DISCUSSION

Synthesis. Complexes **1** and **2**·H_2O were synthesized by the reaction of $K[Au(CN)_2]$, MebptH, and $FeSO_4·7H_2O$. It should be noted that the synthesis conditions for **1** were similar to those for **2**·H_2O except for the solvent proportion and reaction temperature. Indeed, they simultaneously exist in the Teflon-lined reactor with different amount. In the optimized condition given in the Experimental Section, **1** is dominant with higher temperature and ethanol/water ratio with a small amount of **2**·H_2O, and vice versa. This may be attributed to the solvent polarity and/or the different potential energy of the *trans* and *cis* configuration. Since **1** is dark-red in block shape and **2**·H_2O is yellow in prism at room temperature as shown in Figure 1, we can manually separate them under microscope. The TG analysis indicates that **2**·H_2O is stable up to 413 K (Supporting Information Figure S3), while further heating causes a two-step dehydration centered at 456 and 569 K to yield new complex **2**. The DSC curve also shows two endothermic peaks centered at 449 and 574 K (Supporting Information Figure S4), corresponding to the two-step dehydration process. The variable-temperature PXRD spectra for **2**·H_2O from 298 to 598 K confirms the preservation of the framework structure of complex **2**·H_2O upon dehydration, so the Fe(II) centers in **2** are in *trans* configurations as well. Furthermore, the identical chemical compositions between **1** and **2** make them genuine supramolecular isomers.[7b]

Crystal Structures. Single crystal X-ray diffraction analysis reveals that complex **1** crystallizes in the monoclinic space group $C2/c$ (Table 1). There are two crystallographically independent sites Fe1 and Fe2, which are both located in N_6 octahedral environment provided by two $Mebpt^-$ ligands and two $[Au(CN)_2]^-$. However, their coordination configurations are different, namely *trans* configuration around Fe1 while *cis* configuration around Fe2 (Scheme 1a). In addition, the triazole group (N2) and the pyridyl moiety (N1) coordinate to Fe1, forming a dihedral angle of 11.71° between respective planes. Also, another dihedral angle formd by the triazole group (N4) and the Me-pyridyl moiety coordinating (N5) to Fe2 is 17.73°. The Fe1 and Fe2 units are connected by the $Mebpt^-$ ligand in *trans* bridging mode, giving rise to a 1D $[Fe(Mebpt)]^+$ chain (Figure 1a). Then, the $[Au(CN)_2]^-$ groups connect the two iron sites in an alternate way, defining a corrugated 2D $[Fe(Mebpt)\{Au(CN)_2\}]_n$ layer (Figure 1b). They are further packed into three-dimensional supramolecular structures through interlayer edge-to-face $\pi\cdots\pi$ interactions (Figure 2). It is interesting to note that **1** gives the first example with both *cis* and *trans* configurations captured in a 2D coordination polymer. At 373 K, the average Fe−N bond lengths (Table 2) are 2.164 (16) and 2.193 (16) Å for Fe1 and Fe2, respectively, indicating both Fe1 and Fe2 are in HS states. Upon cooling to 150 K, the corresponding values decrease sizably to 1.995 (8) Å at the Fe1 site, whereas it decreases only marginally to 2.175(3) Å at Fe2 site. The change of 0.169 Å in the Fe1−N length, accompanying a clear crystal color change from red to black (Figure 4a), suggests an HS to LS transition upon the temperature change,[13] while Fe2−N is hardly changed, indicating a preservation of HS state. These are also supported by the distortion parameters of the Fe^{II} octahedral sphere. The Σ_{Fe1} values are 67.6°/47.6° at 373/150 K, respectively, whereas the Σ_{Fe2} values are 85.6°/84.8° at 373/150 K, respectively, in accordance with smaller Σ in the LS state and bigger Σ in the HS state.[13]

Complex **2**·H_2O is a generalized supramolecular isomer of **1** disregarding the H_2O in the cavity, and it crystallizes in the triclinic space group $P\bar{1}$ (Table 1). There is one crystallo-

dx.doi.org/10.1021/ic402096s | *Inorg. Chem.* 2014, 53, 201−208

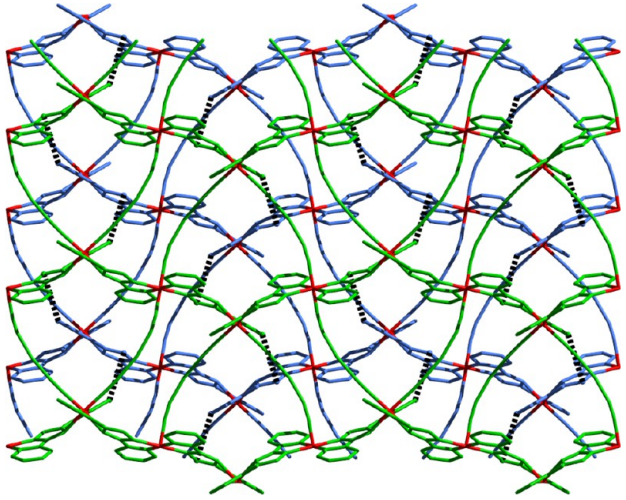

Figure 2. Structural illustrations of **1**: crystal packing of two adjacent 2D layers highlighting the interchains' C−H···N (black dashed lines) interactions. Hydrogen atoms have been omitted for clarity.

graphically independent site Fe1 that is located in N_6 octahedral environment provided by two Mebpt$^-$ ligands and two $[Au(CN)_2]^-$ in *trans* configuration. The Mebpt$^-$ ligand is closer to planar, with two dihedral angle is 5.54° [the triazole group (N3) and the pyridyl moiety (N4)] and 5.86° [the triazole group (N2) and the Me-pyridyl moiety (N1)], respectively. The Mebpt$^-$ ligand connects two Fe1 centers in *cis* bridging mode (Scheme 1b) forming a dinuclear $[Fe(Mebpt)]^{2+}$ unit (Figure 1c). Then they are connected by two $[Au(CN)_2]^-$ bridges, defining a ladder 1D chain (Figure 1d). Consecutive chains are further packed into three-dimensional supramolecular structures through interchains face-to-face $\pi\cdots\pi$ and C−H···N interactions (Figure 3). There are voids between the chains which contain interstitial water molecules. Though they have no obvious hydrogen bond interaction with the coordination frameworks, their disordered position in two positions can be determined from the crystal structure at 150 K, while at 275 and 350 K the increasing severe disorder rules out the possibility for exact assignment of the residual Q peaks; thus, they are removed by SQUEEZE.[14b] The average Fe−N bond lengths at 350, 275, and 150 K (Table 2) are 2.173(16), 2.069(3), and 1.975(11) Å, respectively. The total Fe1−N change between 350 and 150 K is equal to 0.198 Å, accompanying with a clear crystal color change from orange to black (Figure 4b). The variations of the Σ value are comparable with the change of Fe−N length decrease from 109.3° at 350 K to 52.1° at 150 K via 85.2° at 275 K, in accordance with bigger Σ in the HS state and smaller Σ in the LS state.[13]

Magnetic Properties. At 375 K, the $\chi_m T$ value of **1** is 3.59 cm^3 K mol^{-1} (Figure 4a), suggesting all of the Fe(II) centers (*cis* and *trans*) are in the HS state. As the temperature is lowered, $\chi_m T$ first remains almost constant and then decreases to a plateau at ca. 225 K (1.94 cm^3 K mol^{-1}), indicating only half of the Fe(II) ions undergo SCO at T_c = 303 K. Below 175 K, $\chi_m T$ is nearly constant until 30 K. A further drop of $\chi_m T$ below 30 K is due to the occurrence of zero-field splitting on the residual HS iron sites. This is consistent with the structure determination (only Fe(II) in *trans* configuration is SCO active). The $\chi_m T$ versus T plot for **1** suggests a rare example of mixed spins at low temperature,[15] and a thermal induced broad half-SCO.[16] No hysteresis loop was observed in the temperature-dependent susceptibility measurements.

The $\chi_m T$ value of **2**·H_2O at 350 K is 3.56 cm^3 K mol^{-1} (Figure 4b), in agreement with all Fe(II) in the HS state. Then it decreases gradually on cooling to 3.35 cm^3 K mol^{-1} at 325 K and then descends more rapidly to 2.01 cm^3 K mol^{-1} at 275 K. Below 275 K, the $\chi_m T$ value continuously decreases to reach 0.74 cm^3 K mol^{-1} at 190 K, indicating Fe(II) is close to the LS state. A close examination of the temperature dependence of $d\chi T/dT$ curve revealed that the magnetic curve changes its slope with two maxima at 235 and 313 K, respectively.[17] The short plateau is practically reduced to an inflection point approximately at 275 K, and indicates about 50% of the complexes undergoing a thermal spin conversion. These results suggest that **2**·H_2O undergoes gradual two-step SCO.

The dehydrated complex **2** shows a slow spin transition behavior with the $\chi_m T$ value of 3.33 cm^3 K mol^{-1} at 360 K (Figure 4c). Upon cooling to 250 K, the $\chi_m T$ drops to 1.27 cm^3 K mol^{-1}, then decreases slowly to 0.67 cm^3 K mol^{-1} at 50 K, which indicates a gradual one-step SCO with T_c = 315 K.

DSC analyses are performed as shown in Figure 5. For complex **1**, DSC curves display one abnormal peak at T_c = 303 K, which is consistent with the magnetic data. The transition enthalpy (H) and entropy (S) are ΔH = 7.6 kJ mol^{-1} and ΔS =

Table 2. Selected Bond Lengths (Å) and Structural Parameters of 1 and 2·H_2O at Various Temperatures

	1 (150K)	**1** (373K)		**2**·H_2O (150 K)	**2**·H_2O (275 K)	**2**·H_2O (350 K)
Fe(1)−N(1)	2.025(8)	2.194(17)	Fe(1)−N(1)	2.095(12)	2.143(14)	2.260(14)
Fe(1)−N(2)	2.025(8)	2.135(15)	Fe(1)−N(2)	1.905(10)	2.010(12)	2.026(16)
Fe(1)−N(6)	1.955(8)	2.160(17)	Fe(1)−N(3)	1.920(11)	2.002(12)	2.135(12)
Fe(2)−N(4)	2.170(8)	2.164(14)	Fe(1)−N(4)	2.071(12)	2.149(14)	2.254(17)
Fe(2)−N(5)	2.193(9)	2.251(16)	Fe(1)−N(6)	1.936(10)	2.062(14)	2.210(15)
Fe(2)−N(7)	2.144(9)	2.194(13)	Fe(1)−N(7)	1.920(10)	2.047(13)	2.151(13)
Fe(1)−Fe(2)	5.880(2)	5.980(2)	Fe(1)−Fe(1)	4.000(7)	4.190(3)	4.244(6)
Au(1)−Au(1)	3.5714(9)	3.745(2)		3.965(8)	4.491(5)	4.897(6)
$\langle d$Fe1−N$\rangle^a$	1.995(8)	2.164(16)		1.975	2.069	2.173
$\langle d$Fe2−N$\rangle^a$	2.175(8)	2.193(16)				
$\sum_{Fe1}$ (deg)	47.6	67.6		52.1	85.2	109.3
$\sum_{Fe2}$ (deg)	84.8	85.6				
$\pi\cdots\pi$ distance (Å)	4.070	4.072		3.625	3.775	3.818
C−H···N hydrogen bonds	3.426	3.441		3.439	3.447	3.474

[a] $\langle d$Fe−N$\rangle$ is the average Fe−N distance.

dx.doi.org/10.1021/ic402096s | *Inorg. Chem.* 2014, 53, 201−208

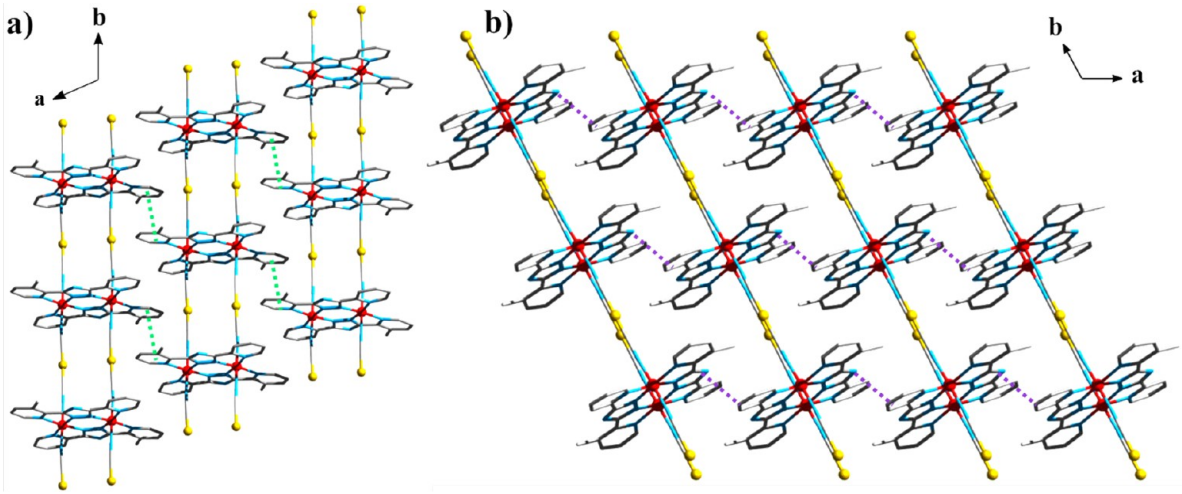

Figure 3. Structural illustrations of **2**·H_2O: crystal packing of two adjacent 1D chains highlighting the interchains face to face $\pi\cdots\pi$ (green dashed lines) interactions (a) and the interchains' C−H···N (purple dashed lines) interactions (b). Hydrogen atoms have been omitted for clarity.

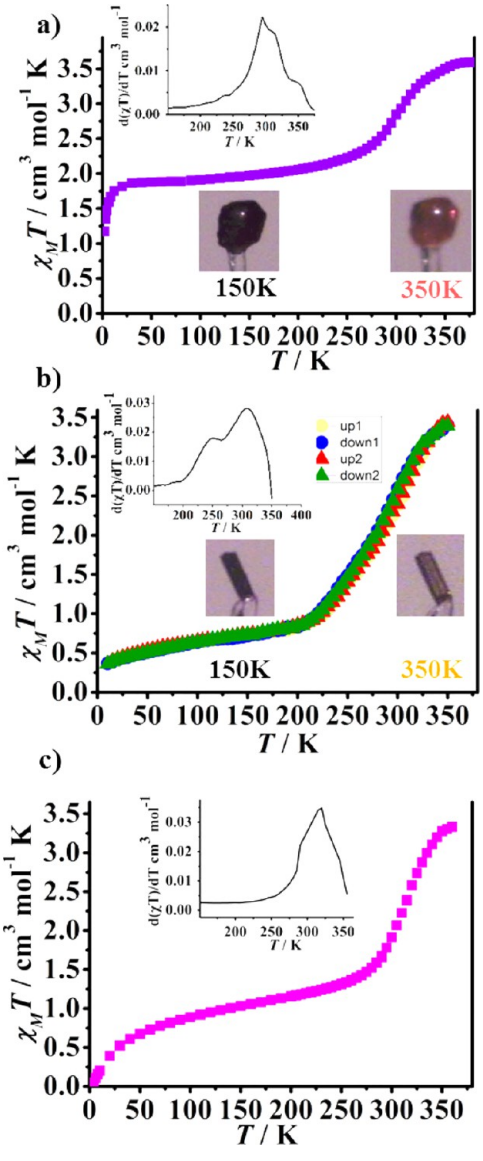

Figure 4. $\chi_m T$ vs T of **1** (purple ■) (a), **2**·H_2O (blue ■) (b), and **2** (magenta ■) (c). The inset shows the first derivative of χT.

25.2 J K^{-1} mol^{-1}, respectively. For complex **2**·H_2O, DSC curves display two abnormal peaks at T_{c1} = 235 K, and T_{c2} = 313 K, corresponding to the occurrence of two-step SCO. The enthalpy and entropy variations are ΔH_1 = 3.7 kJ mol^{-1}, ΔH_2 = 6.3 kJ mol^{-1}, and ΔS_1 = 15.8 J K^{-1} mol^{-1}, ΔS_2 = 19.7 J K^{-1} mol^{-1}, respectively. The overall variations are ΔH = 10.0 kJ mol^{-1} and ΔS = 35.5 J K^{-1} for **2**·H_2O. For complex **2**, DSC curves display one abnormal peak at T_c = 315 K, which is consistent with the magnetic data. The transition enthalpy (H) and entropy (S) are ΔH = 14.0 kJ mol^{-1} and ΔS = 44.3 J K^{-1} mol^{-1}, respectively. The overall variations are within the experimental range generally observed for Fe(II) SCO complexes.[18a]

Comparison of the Magnetic Properties of Isomers 1 and 2·H_2O. Supramolecular isomers in SCO systems with different magnetic properties were discovered in many cases,[8] which is often possibly attributed to dissimilar crystal packings in different polymorphs. However, a direct elucidation of the spin-transition properties from a careful structural analysis is a difficult task because the subtle changes of intermolecular interactions may result in radically different transition behaviors. In the present situation, we offer a deep insight into the structural−magneto relationship of two isomers based on the $[Fe(Mebpt)\{Au(CN)_2\}]_n$ system. Selected bond lengths and structural parameters of the supramolecular isomers are listed in Table 2. On closer inspection of **1** and **2**·H_2O, we can see that the great differences in the structures result in a prominent discrepancy in their magnetic properties. The *cis* configuration Fe(II) centers in **1** remain in the HS state at all probed temperatures, while the Fe(II) centers in the *trans* configuration in **1** and **2**·H_2O exhibit reversible spin transitions near room-temperature. First, this can be ascribed to the difference between the dihedral angles formed by the triazole with adjacent aromatic moieties in **1** (respectively, 11.71° and 17.73°), which may influence the ligand field strength through the conjugation effect, in accordance with the electron density value calculated from the crystallography (Figure 6) where N2 has higher electron density compared with N4.[18b−d] Second, a slightly shorter *trans* Fe1−N bond length (Table 2) should play a role in its transition, taking into account that the ligand field strength, Δ_0, is proportional to $1/R^6$ (Fe−N bond distances); a decrease of *ca.* 7.7% can be estimated for Fe1 with respect to

dx.doi.org/10.1021/ic402096s | *Inorg. Chem.* 2014, 53, 201−208

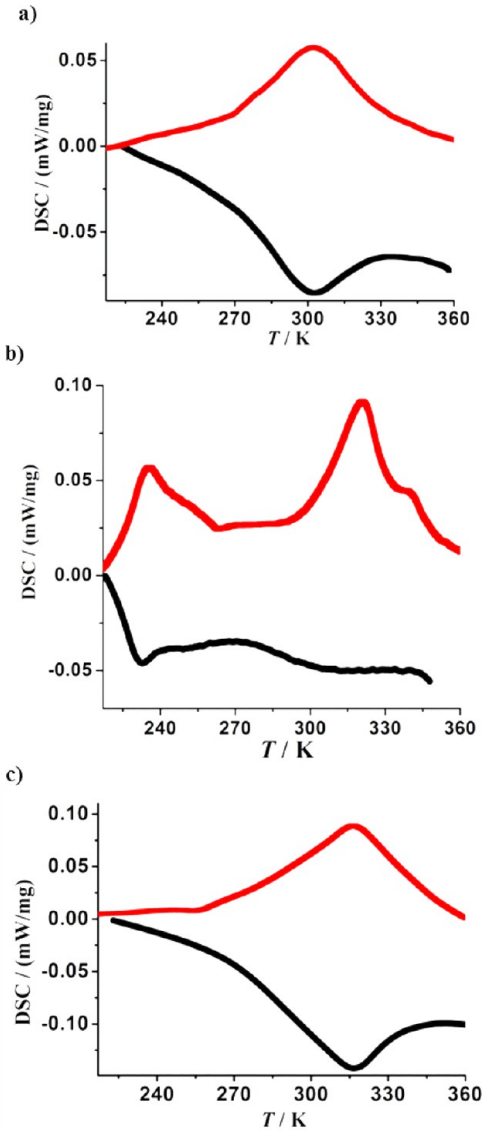

Figure 5. DSC curves of **1** (a), **2**·H_2O (b), and **2** (c) corresponding to the spin transitions. The traces measured in the heating and cooling modes are colored in red and black, respectively. Cooling/heating rates: 5 K min^{-1}.

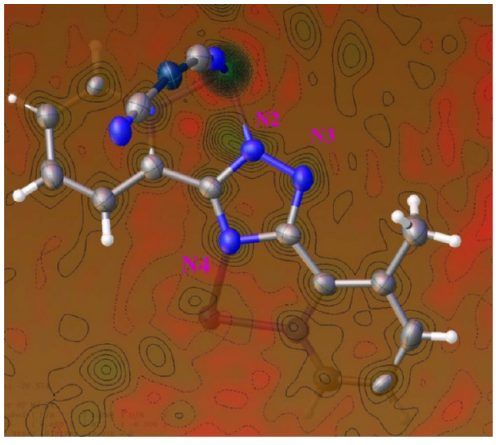

Figure 6. Electron density maps for **1** at 150 K.

Fe2.[18e] These indicate that the observation of SCO in **1** relies on the presence of the *trans* configuration providing an optimized ligand field.[9b] It is also true for **2**·H_2O, where the ligand in **2**·H_2O is closer to planar and thus has stronger conjugation effects (see structural description above). Therefore, **2**·H_2O undergoes more complete two-step SCO with an intermediate phase which may be due to the formation of a 50% mixture of [HS−HS] and [LS−LS] or to the existence of 100% [LS−HS] species (Figure 4b).[19a,b] Although no crystallographic evidence for symmetry breaking was captured, the possibility cannot be ruled out, because the structural changes might be too subtle to be detected by X-ray diffraction.[19c,d] Previously, a similar effect was also observed in another Fe(II) complex based on triazole deriving ligands and showing gradual two-step spin transition.[17b]

In order to understand the nature of the different behavior of the Fe^{II} centers in the studied complexes, a theoretical study using DFT methods was carried out.[20] Calculations were performed using the Gaussian09 code[21] with the OPBE exchange-correlation functional[22a,b] and the TZVP all electron basis set.[22c] The OPBE functional provide excellent results for the calculation of the energy difference between spin states.[22d] Two different kinds of systems were considered in the calculations: (i) The first was dinuclear Fe complexes using the X-ray (see Figure 1) data to estimate the energy differences between high and low spin states replacing one of the Fe^{II} centers by a diamagnetic Zn^{II} cation. Thus, the energy difference can be determined for each Fe^{II} center present in the structure. (ii) The second was optimized geometries for dianionic mononuclear Fe^{II} complexes including the $[Au(CN)_2]^-$ and $Mebpt^-$ ligands.

DFT calculations of the relative stability of the high and low spin states for the X-ray dinuclear FeZn systems for **1** and **2** (see Figure 1a,c and details on computational studies) are consistent with the observed spin transition of the *trans* bridged moieties and with the lack of transition of the **1***cis* fragment. The *trans* models for **1** and **2** present a switch of the most stable state from the low spin state at low temperature structure to the high temperature geometry, where the high spin is favored. On the other hand, the high spin state is always the most stable solution for the **1***cis* conformation, independent of the temperature (Table 3).

Table 3. DFT Calculated Relative Stability of High and Low Spin States[a] for the X-ray Determined Structures at Different Temperatures[b]

	T (K)		
model	150	298 (**1**), 275 (**2**)	373 (**1**), 350 (**2**)
1*trans*	111.1	7.4	−90.1
1*cis*	−103.5	−122.2	−119.6
2*trans*	146.8	−6.2	−110.6

[a] $E_{HS\text{-}LS}$ in kJ mol^{-1}, negative value means HS is more stable. [b] Low: 150 K for **1** and **2**. Intermediate: 298 K for **1**, 275 K for **2**. High: 373 K for **1**, 350 K for **2**.

Differences in spin transition between **1***trans* and **1***cis* mononuclear Fe^{II} models were further investigated by structural optimization for both models. These kinds of geometry optimizations are done at 0 K; thus, spin-crossover systems have low spin state as ground state. The increase of temperature will compensate for such high and low spin energy differences through the vibrational and electronic

dx.doi.org/10.1021/ic402096s | Inorg. Chem. 2014, 53, 201−208

entropic terms. An estimation of the limit of energy difference at 0 K, that can be overcome by such entropic effects, to have the low−high spin transition at 300 K, is around 35 kJ mol^{-1}. The high spin−low spin energy gap including zero-point vibrational energy corrections for **1***trans* is 22.3 kJ mol^{-1}; this value is in the expected interval for compounds with spin transition. On the other hand, **1***cis* presents a much smaller gap (4.84 kJ/mol), in line with the observed stability of the high spin state for the studied temperature range.

The energy and shape of the orbitals with five Fe d-orbital contribution can give more insight into the origin of the different behavior of **1***trans* and **1***cis* (see Figure 7). The analysis

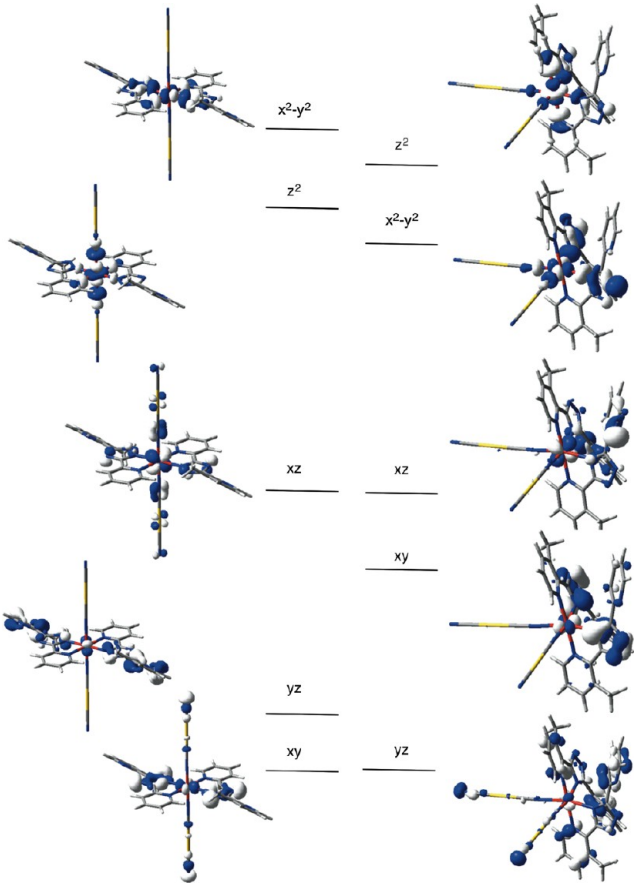

Figure 7. Splitting of the five 3d orbitals of the optimized ***1trans*** and ***1cis*** systems.

of the **1***trans* orbitals indicates that the antibonding orbitals containing the $[Au(CN)_2]^-$ ligand are more stable than that corresponding to the $Mebpt^-$ ligands. It is worth keeping in mind that the nitrogem atom coordinated to the metal of the 1,2,4-triazole group of the $Mebpt^-$ ligand changes from N2 to N1 for the **1***trans* and **1***cis*, respectively. The main difference is the relative stability of the *xy* orbital, in that the **1***cis* system becomes more π-antibonding (stronger π interaction with the N1 of the triazole) in comparison with the **1***trans* complex. This fact reduces the stability of the low spin state for the **1***cis* system, in agreement with the lack of spin transition of the high spin Fe^{II} centers with *cis* coordination. Also, favoring the high spin state of the **1***cis* system, the M−L antibonding orbitals (z^2 and $x^2 - y^2$) are more stable than those corresponding to the **1***trans* coordination.

CONCLUSION

In this study, two interesting spin crossover supramolecular isomers formulated as $[Fe(Mebpt)\{Au(CN)_2\}]_n$ were obtained from the hydrothermal reactions of $FeSO_4$, 3-(5-methyl-2-pyridyl)-5-(2-pyridyl)-1,2,4-triazole (MebptH), and $KAu(CN)_2$. It is interesting to note that subtle changes in the bridging modes of the ligands lead to entirely different structural architectures and the coordination configuration of Fe(II) and, thus, distinct magnetic properties. Isomer **1** represents the first Fe(II) based 2D coordination polymer with both *cis* and *trans* configurations, in which only the Fe(II) centers in *trans* configuration could change the spin state (T_c = 303 K). While all the Fe(II) centers of **2**·H_2O are in *trans* configurations and show gradual two-step SCO behavior (T_{c1} = 235 K, T_{c2} = 313 K), the dehydration product **2** exhibits one-step SCO (T_c = 315 K). DFT results corroborate that the *cis* coordination favors the high spin state while *trans* coordination promotes the spin-crossover behavior.

ASSOCIATED CONTENT

Supporting Information

Photographs of **1** and **2**·H_2O, TG curves for **2**·H_2O and **2**, DSC curves for **2**·H_2O, powder X-ray diffraction patterns for **1**, and variable PXRD patterns for **2**·H_2O. This material is available free of charge via the Internet at http://pubs.acs.org.

AUTHOR INFORMATION

Corresponding Authors

*E-mail: tongml@mail.sysu.edu.cn.
*E-mail: eliseo.ruiz@qi.ub.es.

Notes

The authors declare no competing financial interest.

ACKNOWLEDGMENTS

This work was supported by the "973 Project" (2012CB821704 and 2014CB845602), Program for Changjiang Scholars and Innovative Research Team in University of China, the NSFC (Grants 91122032, 21201182, and 21121061), and the Spanish Ministerio de Economia y Competitividad (CTQ2011-23862-C02-01 and CTQ2012-32247) and the regional Generalitat de Catalunya authority (2009SGR-1459). D.A. thanks the Conicyt (Chile) for a predoctoral fellowship. The authors thankfully acknowledge the computer resources, technical expertise, and assistance provided by the CESCA.

REFERENCES

(1) (a) Gütlich, P.; Goodwin, H. A. Spin Crossover in Transition Metal Compounds I, II and III. *Topics in Current Chemistry*; Springer-Verlag: Berlin, 2004; Vol. *233*. (b) Kahn, O.; Martinez, C. J. *Science* **1998**, *279*, 44.

(2) (a) Real, J. A.; Andrés, E.; Muñoz, M. C.; Julve, M.; Granier, T.; Bousseksou, A.; Varret, F. *Science* **1995**, *268*, 265. (b) Bousseksou, A.; Molnár, G.; Salmon, L.; Nicolazzi, W. *Chem. Soc. Rev.* **2011**, *40*, 3313. (c) Halcrow, M. A. *Chem. Soc. Rev.* **2011**, *40*, 4119. (d) Guionneau, P.; Marchivie, M.; Bravic, G.; Létard, J.-F.; Chasseau, D. *Top. Curr. Chem.* **2004**, *234*, 97. (e) Sato, O.; Tao, J.; Zhang, Y.-Z. *Angew. Chem., Int. Ed.* **2007**, *46*, 2152. (f) Murray, K. S. In *Spin-Crossover Materials*; John Wiley & Sons Ltd.: New York, 2013; p 1.

(3) (a) Bousseksou, A.; Molnár, G.; Salmon, L.; Nicolazzi, W. *Chem. Soc. Rev.* **2011**, *40*, 3313. (b) Létard, J.-F.; Guionneau, P.; Goux-Capes, L. *Top. Curr. Chem.* **2004**, *235*, 221.

(4) (a) Halder, G. J.; Kepert, C. J.; Moubaraki, B.; Murray, K. S.; Cashion, J. D. *Science* **2002**, *298*, 1762. (b) Ohba, M.; Yoneda, K.;

Agustí, G.; Muñoz, M. C.; Gaspar, A. B.; Real, J. A.; Yamasaki, M.; Ando, H.; Nakao, Y.; Sakaki, S.; Kitagawa, S. *Angew. Chem., Int. Ed.* **2009**, *48*, 4767. (c) Bressler, C.; Milne, C.; Pham, V.-T.; ElNahhas, A.; van der Veen, R. M.; Gawelda, W.; Johnson, S.; Beaud, P.; Grolimund, D.; Kaiser, M.; Borca, C. N.; Ingold, G.; Abela, R.; Chergui, M. *Science* **2009**, *323*, 489. (d) Venkataramani, S.; Jana, U.; Dommaschk, M.; Sönnichsen, F. D.; Tuczek, F.; Herges, R. *Science* **2011**, *331*, 445. (e) Ohkoshi, S.; Imoto, K.; Tsunobuchi, Y.; Takano, S.; Tokoro, H. *Nat. Chem.* **2011**, *3*, 564. (f) Hoshino, N.; Iijima, F.; Newton, G. N.; Yoshida, N.; Shiga, T.; Nojiri, H.; Nakao, A.; Kumai, R.; Murikami, Y.; Oshio, H. *Nat. Chem.* **2012**, *4*, 921. (g) Yan, Z.; Li, M.; Gao, H.-L.; Huang, X.-C.; Li, D. *Chem. Commun.* **2012**, *48*, 3960.

(5) Murray, K. S.; Kepert, C. J. *Top. Curr. Chem.* **2004**, *233*, 195.

(6) (a) Garcia, Y.; Niel, V.; Muñoz, M. C.; Real, J. A. *Top. Curr. Chem.* **2004**, *233*, 229. (b) Weber, B.; Bauer, W.; Obel, J. *Angew. Chem., Int. Ed.* **2008**, *52*, 10098.

(7) (a) Moulton, B.; Zaworotko, M. J. *Chem. Rev.* **2001**, *101*, 1629. (b) Zhang, J.-P.; Huang, X.-C.; Chen, X.-M. *Chem. Soc. Rev.* **2009**, *38*, 2385.

(8) Tao, J.; Wei, R.-J.; Huang, R. B.; Zheng, L. S. *Chem. Soc. Rev.* **2012**, *41*, 703.

(9) (a) Bréfuel, N.; Duhayon, C.; Shova, S.; Tuchagues, J.-P. *Chem.Commun.* **2007**, 5223. (b) Kitchen, J. A.; Jameson, G. N. L.; Tallon, J. L.; Brooker, S. *Chem. Commun.* **2010**, *46*, 3200.

(10) (a) Klingele, M. H.; Brooker, S. *Coord. Chem. Rev.* **2003**, *241*, 119. (b) Kitchen, J. A.; Brooker, S. *Coord. Chem. Rev.* **2008**, *252*, 2072. (c) Peng, M.-X.; Hong, C.-G.; Tan, C.-K.; Chen, J.-C.; Tong, M.-L. *J. Chem. Crystallogr.* **2006**, *36*, 703. (d) Chen, J.-C.; Hu, S.; Zhou, A.-J.; Tong, M.-L.; Tong, Y.-X. *Z. Anorg. Allg. Chem.* **2006**, *632*, 475. (e) Tong, M.-L.; Hong, C.-G.; Zheng, L.-L.; Peng, M.-X.; Gaita-Ariño, A.; Clemente Juan, J. M. *Eur. J. Inorg. Chem.* **2007**, 3710. (f) Meng, Z.-S.; Yun, L.; Zhang, W.-X.; Hong, C.-G.; Herchel, R.; Ou, Y.-C.; Leng, J.-D.; Peng, M.-X.; Lin, Z.; Tong, M.-L. *Dalton Trans.* **2009**, 10284. (g) Bao, X.; Leng, J.-D.; Meng, Z.-S.; Lin, Z.-J.; Tong, M.-L.; Nihei, M.; Oshio, H. *Chem.—Eur. J.* **2010**, *16*, 6169. (h) Bao, X.; Liu, J.-L; Leng, J.-D.; Lin, Z.-J.; Tong, M.-L.; Nihei, M.; Oshio, H. *Chem.—Eur. J.* **2010**, *16*, 7973. (i) Bao, X.; Guo, P.-H.; Liu, J.-L; Leng, J.-D.; Tong, M.-L. *Chem.—Eur. J.* **2011**, *17*, 2335.

(11) (a) Niel, V.; Thompson, A. L.; Muñoz, M. C.; Galet, A.; Goeta, A. E.; Real, J. A. *Angew. Chem., Int. Ed.* **2003**, *42*, 3760. (b) Galet, A.; Muñoz, M. C.; Martínez, V.; Real, J. A. *Chem. Commun.* **2004**, 2268. (c) Galet, A.; Muñoz, M. C.; Real, J. A. *Chem. Commun.* **2006**, 4321. (d) Agustí, G.; Muñoz, M. C.; Gaspar, A. B.; Real, J. A. *Inorg. Chem.* **2008**, *47*, 2552. (e) Agustí, G.; Gaspar, A. B.; Muñoz, M. C.; Lacroix, P. G.; Real, J. A. *Aust. J. Chem.* **2009**, *62*, 1155. (f) Kosone, T.; Kanadani, C.; Saito, T.; Kitazawa, T. *Polyhedron* **2009**, *28*, 1991. (g) Kosone, T.; Tomori, I.; Kanadani, C.; Saito, T.; Mochida, T.; Kitazawa, T. *Dalton Trans.* **2010**, *39*, 1719. (h) Kosone, T.; Kachi-Terajima, C.; Kanadani, C.; Saito, T.; Kitazawa, T. *Chem. Lett.* **2008**, *37*, 422.

(12) Muñoz-Lara, F. J.; Gaspar, A. B.; Muñoz, M. C.; Lysenko, A. B.; Domasevitch, K. V.; Real, J. A. *Inorg. Chem.* **2012**, *51*, 13078.

(13) Guionneau, P.; Marchivie, M.; Bravic, G.; Létard, J.-F.; Chasseau, D. *Top. Curr. Chem.* **2004**, *234*, 97.

(14) (a) Sheldrick, G. M. *Acta Crystallogr.* **2008**, *A64*, 112. (b) van der Sluis, P.; Spek, A. L. *Acta Crystallogr.* **1990**, *A46*, 194. (c) Spek, A. L. *J. Appl. Crystallogr.* **2003**, *36*, 7.

(15) Li, F.; Clegg, J. K.; Goux-Capes, L.; Chastanet, G.; D'Alessandro, D. M.; Létard, J.-F.; Kepert, C. J. *Angew. Chem., Int. Ed.* **2011**, *50*, 2820.

(16) Grunert, C. M.; Reiman, S.; Spiering, H.; Kitchen, J. A.; Brooker, S.; Gütlich, P. *Angew. Chem., Int. Ed.* **2008**, *47*, 2997.

(17) (a) Vieira, B. J. C.; Coutinho, J. T.; Santos, I. C.; Pereira, L. C. J.; Waerenborgh, J. C.; da Gama, V. *Inorg. Chem.* **2013**, *52*, 3845. (b) Dupouy, G.; Triki, S.; Marchivie, M.; Cosquer, N.; Gómez-García, C. J.; Pillet, S.; Bendeif, E.-E.; Lecomte, C.; Asthana, S.; Létard, J.-F. *Inorg. Chem.* **2010**, *49*, 9358.

(18) (a) Šalitroš, I.; Madhu, N. T.; Boča, R.; Pavlik, P.; Ruben, M. *Monatsh. Chem.* **2009**, *140*, 695. (b) Gütlich, P.; Garcia, Y.; Goodwin, H. A. *Chem. Soc. Rev.* **2000**, *29*, 419. (c) Bao, X.; Guo, P.-H.; Liu, W.; Tucek, J.; Zhang, W. X.; Leng, J. D.; Chen, X. M.; Gural'skiy, I.; Salmon, L.; Bousseksou, A.; Tong, M.-L. *Chem. Sci.* **2012**, *3*, 1629. (d) Dolomanov, O. V.; Bourhis, L. J.; Gildea, R. J.; Howard, J. A. K.; Puschmann, H. *J. Appl. Crystallogr.* **2009**, *42*, 339. (e) Tayagaki, T.; Galet, A.; Molnr, G.; Muñoz, M. C.; Zwick, A.; Tanaka, K.; Real, J. A.; Bousseksou, A. *J. Phys. Chem. B* **2005**, *109*, 14859.

(19) (a) Gaspar, A. B.; Muñoz, M. C.; Real, J. A. *J. Mater. Chem.* **2006**, *16*, 2522. (b) Bousseksou, A.; Molnár, G.; Real, J. A.; Tanaka, K. *Coord. Chem. Rev.* **2007**, *251*, 1822. (c) Bao, X.; Shepherd, H. J.; Salmon, L.; Molnár, G.; Tong, M.-L.; Bousseksou, A. *Angew. Chem., Int. Ed.* **2013**, *52*, 1198. (d) Chernyshov, D.; Hostettler, M.; Törnroos, K. W.; Bürgi, H.-B. *Angew. Chem., Int. Ed.* **2003**, *42*, 3825.

(20) (a) Paulsen, H.; Schuenemann, V.; Wolny, J. A. *Eur. J. Inorg. Chem.* **2013**, 628. (b) Kepp, K. P. *Coord. Chem. Rev.* **2013**, *257*, 196. (c) Deeth, R. J.; Handley, C. M.; Houghton, B. J. In *Spin-Crossover Materials*; John Wiley & Sons Ltd.: New York, 2013; p 443.

(21) Frisch, M. J.; Trucks, G. W.; Schlegel, H. B.; Scuseria, G. E.; Robb, M. A.; Cheeseman, J. R.; Scalmani, G.; Barone, V.; Mennucci, B.; Petersson, G. A.; Nakatsuji, H.; Caricato, M.; Li, X.; Hratchian, H. P.; Izmaylov, A. F.; Bloino, I. J.; Zheng, G.; Sonnenberg, J. L.; Hada, M.; Ehara, M.; Toyota, K.; Fukuda, R.; Hasegawa, J.; Ishida, M.; Nakajima, T.; Honda, Y.; Kitao, O.; Nakai, H.; Vreven, T.; Montgomery, J. J. A.; Peralta, J. E.; Ogliaro, F.; Bearpark. M.; Heyd, J. J.; Brothers, E.; Kudin, K. N.; Staroverov, V. N.; Kobayashi, R.; Normand, J.; Raghavachari, K.; Rendell, A.; Burant, J. C.; Iyengar, S. S.; Tomasi, J.; Cossi, M.; Rega, N.; Millam, J. M.; Klene, M.; Knox, J. E.; Cross, J. B.; Bakken, V.; Adamo, C.; Jaramillo, J.; Gomperts, R.; Stratmann, R. E.; Yazyev, O.; Austin, A. J.; Cammi, C.; Pomelli, J. W.; Ochterski, R.; Martin, R. L.; Morokuma, K.; Zakrzewski, V. G.; Voth, G. A.; Salvador, P.; Dannenberg, J. J.; Dapprich, S.; Daniels, A. D.; Farkas, O.; Foresman, J. B.; Ortiz, J. V.; Cioslowski, J.; Fox, D. J. *Gaussian 09, Revision A.1*; Gaussian: Wallingford, CT, 2009.

(22) (a) Handy, N. C.; Cohen, A. *J. Mol. Phys.* **2001**, *99*, 403. (b) Perdew, J. P.; Burke, K.; Ernzerhof, M. *Phys. Rev. Lett.* **1996**, *77*, 3865. (c) Schaefer, A.; Huber, C.; Ahlrichs, R. *J. Chem. Phys.* **1994**, *100*, 5829. (d) Swart, M. *J. Chem. Theory Comput.* **2008**, *4*, 2057.